Australasian Physical & Engineering Sciences in Medicine (2019) 42:181–190
https://doi.org/10.1007/s13246-019-00728-7

SCIENTIFIC PAPER

Computational study on hemodynamic changes in patient-specific proximal neck angulation of abdominal aortic aneurysm with time-varying velocity

Yousif A. Algabri[1] · Sorracha Rookkapan[2] · Vera Gramigna[3] · Daniel M. Espino[4] · Surapong Chatpun[1]

Received: 10 July 2018 / Accepted: 21 January 2019 / Published online: 14 February 2019

Abstract

Aneurysms are considered as a critical cardiovascular disease worldwide when they rupture. The clinical understanding of geometrical impact on the flow behaviour and biomechanics of abdominal aortic aneurysm (AAA) is progressively developing. Proximal neck angulations of AAAs are believed to influence the hemodynamic changes and wall shear stress (WSS) within AAAs. Our aim was to perform pulsatile simulations using computational fluid dynamics (CFD) for patient-specific geometry to investigate the influence of severe angular ($\geq 60°$) neck on AAA's hemodynamic and wall shear stress. The patient's geometrical characteristics were obtained from a computed tomography images database of AAA patients. The AAA geometry was reconstructed using Mimics software. In computational method, blood was assumed Newtonian fluid and an inlet varying velocity waveform in a cardiac cycle was assigned. The CFD study was performed with ANSYS software. The results of flow behaviours indicated that the blood flow through severe bending of angular neck leads to high turbulence and asymmetry of flows within the aneurysm sac resulting in blood recirculation. The high wall shear stress (WSS) occurred near the AAA neck and on surface of aneurysm sac. This study explained and showed flow behaviours and WSS progression within high angular neck AAA and risk prediction of abdominal aorta rupture. We expect that the visualization of blood flow and hemodynamic changes resulted from CFD simulation could be as an extra tool to assist clinicians during a decision making when estimation the risks of interventional procedures.

Keywords Abdominal aortic aneurysm · Angulated neck · Computational fluid dynamics · Wall shear stress · Hemodynamic · Computed tomography

Abbreviations

3D	Three-dimensional
AAAs	Abdominal aortic aneurysms
CAD	Computer-aided design
CFD	Computational fluid dynamics
CT	Computed tomography
CVD	Cardiovascular disease
DICOM	Digital imaging and communications in medicine
EVAR	Endovascular aortic aneurysm repair
ILT	Intraluminal thrombus
MR	Magnetic resonance
ROI	Region of interest
STL	Stereolithography
UDF	User-defined function
WSS	Wall shear stress

Electronic supplementary material The online version of this article (https://doi.org/10.1007/s13246-019-00728-7) contains supplementary material, which is available to authorized users.

✉ Surapong Chatpun
surapong.c@psu.ac.th

[1] Institute of Biomedical Engineering, Faculty of Medicine, Prince of Songkla University, 6th floor, 100-year Building, Hatyai, Songkhla 90110, Thailand

[2] Department of Radiology, Faculty of Medicine, Prince of Songkla University, Hatyai, Songkhla 90110, Thailand

[3] Neuroscience Research Center, University Magna Graecia, 88100 Catanzaro, Italy

[4] Department of Mechanical Engineering, University of Birmingham, Birmingham B15 2TT, UK

Introduction

Cardiovascular disease (CVD) is one of the foremost common cause of global mortality rate [1]. In 2013, a report of Global Burden of Disease stated that 17.3 million cases of death caused by CVD globally, which accounted approximately 31.5% of total deaths [1, 2]. One of most prevalent cardiovascular diseases is abdominal aortic aneurysm (AAA) [3]. Abdominal aortic aneurysm is defined as a dilatation of the artery that located below the renal arteries [4, 5], with at least a diameter of 30 mm or about 1.5 times the normal size of aorta [6]. Abdominal aortic aneurysms are often diagnosed through the presence of intraluminal thrombus deposition and are linked to the degradation of the connective tissue in the arterial wall, which made up of cell debris and fibrinous blood clots [7]. Abdominal aortic aneurysms are formed due to several mechanisms, including inflammation of immune responses and aortic wall degradation, which are affected by molecular genetics [8, 9]. During the aneurysm formation, a complex blood flow environment and altered wall shear stress distribution are induced. Moreover, AAA is considered life-threatening health condition, which can require urgent surgical intervention [7]. Continuous AAA expansion leads to the decline of aortic wall strength, in which case the wall becomes susceptible to collapse or eventual aortic rupture [10]. Current clinical recommendations are the following; when the AAA diameters reach 55 mm in men and 50 mm in women, with a development rate of 8.0 mm/year, then surgical intervention is necessary [5, 10].

Currently, AAA intervention approaches include open surgery, endovascular aneurysm repair and endovascular aneurysm sealing and the approaches are based on the diameter size of the aneurysm sac with a follow up routines [11–15]. However, the aneurysm diameter is still a poor indicator of rupture since some reported aneurysms with larger diameter remain intact, while aneurysms of a smaller size have been reported to rupture [5, 10, 16]. Thus, AAA rupture is ranked as the 13th leading cause of mortality in the US alone with approximately 15,000 patients every year, and reports of more than 8,000 cases of death in the UK [7, 17]. Furthermore, a ruptured AAA is considered a fatal surgical emergency which has a mortality rate of 90% [18]. The numerous studies conducted on the prediction of rupture and its risks, have proposed several possible AAA rupture factors including asymmetry flow index, maximum aneurysm diameter, age, aortic wall stiffness, mechanical stress, aneurysm growth rate, intraluminal thrombus ratio, smoking, hypertension and high cholesterol [8, 11, 19–21]. However, morphologies such as aortic neck angulation related to adverse events and outcome after endovascular aneurysm repair (EVAR) [22] have often been overlooked.

Generally, magnetic resonance (MR) and a computer tomography (CT) can be used to obtain the anatomy of cardiovascular structures [23, 24]. The resulting images of vasculature are valuable to generate numerical models which can be used to predict mechanical behavior under these conditions. Thus, Computational fluid dynamics (CFD) has been used for cardiovascular research, including flow analysis and calculation of wall shear stress [25–29]. For the study of AAAs, CFD has been implemented in the applications of idealized or patient-specific geometries to assist in predicting the rupture risks [30, 31]. Several studies suggested that a rupture site may be linked with the wall stress, itself dependent on geometric characteristics including surface curvature and the asymmetry of aneurysms [12, 32–37]. There is the potential to address the paucity of research into the influence of neck angulation on AAA disease progression and AAA risk of rupture, through the use of a numerical model.

The aim of this present study was to use a three-dimensional finite volume method for CFD simulation to determine the impact of severe proximal aneurysm neck angulation on the blood flow in AAAs and wall shear stress (WSS) based on a patient-specific AAA geometry.

Materials and methods

Image acquisition

The three-dimensional (3D) vasculature was based on CT images of a single patient with the AAA fully analysed. These images were acquired from radiology department under the approval of Faculty of Medicine Ethics Committee, Prince of Songkla University with number (REC.61-010-25-2). The CT images were obtained in a DICOM format by AQUILION PRIME (Toshiba, Japan) with single slices, rows and columns of 512×512 pixels, a slice thickness of 3 mm and mean pixel spacing of 0.669×0.669. Table 1 presents patient's demographic information including aneurysm length, aneurysm diameter, infrarenal neck length and angle at the proximal neck.

Three-dimensional model reconstruction

The Three-dimensional (3D) smoothed model was generated from DICOM files by using the commercial medical imaging software Mimics v18.0 (Materialise, Belgium). Mimics was used to convert the acquired CT images into a patient specific 3D CAD model. The region of interest (ROI) was segmented by applying grayscale-based thresholding tools. The DICOM images were cropped from the position of the infra-renal aorta towards the bifurcation of common iliac arteries. The artery branches such as parietal and visceral

Table 1 Patient demographics and geometry dimensions

Patient's information	
Gender	Male
Age (years)	74
Weight (kg)	65
Height (cm)	158
Inflow inlet diameter (mm)	25
Proximal Neck diameter (mm)	20
Infrarenal Neck length (mm)	25
Aneurysm length (mm)	68
Aneurysm diameter (mm)	56
Distal left iliac diameter (mm)	8
Distal right iliac diameter (mm)	8
Angle at proximal neck	79°
Whole model length (mm)	258.06

arteries were excluded from the reconstruction to reduce the complexity of the geometry. Owen et al. showed that the error associated with the exclusion of small branches was smaller than the effect of the simple simulation set up [31]. Examples of the thresholding and segmentation processes are shown in Fig. 1a, b. Finally, the 3D smoothed geometry was generated and exported as a binary 'STL (stereolithography)' format as shown in Fig. 1c. The proximal neck angulation of patient's specific model was measured by using Mimics, with measurement provided in Table 1.

Meshing

The geometry was meshed by using the Octree method in ANSYS ICEM v16.2 (ANSYS Inc., USA) for tetrahedral meshing. An inflation at the wall boundary was implemented with five prism layers. The height of first layer was set to 0.1 mm, and next layers grow with a size ratio of 1.2. Quality and smoothing checks were repeatedly performed to ensure a satisfactory mesh. A grid-size independency study was performed using a $\pm 2.5\%$ for peak velocity as the key criterion. The final selected mesh has 2,077,498 elements.

Boundary conditions and material properties

A finite volume method was implemented to solve the Navier–Stokes and continuity equations of the fluid motion under transient conditions in ANSYS FLUENT v16.2 (ANSYS Inc., USA) solver. Blood flow was assumed to be homogeneous, incompressible, and blood was modelled as a Newtonian fluid. These assumptions are adequate in larger arteries with a constant dynamic viscosity and blood density of 0.0035 Pa·s and 1,060 kg/m^3, respectively [38, 39]. Furthermore, an assumption of flow in aorta with >0.5 mm diameter as a Newtonian is acceptable since the viscosity of blood is comparatively constant at the high shear rates (100/s), and this case is typically found in abdominal aortas [40, 41]. For the fluid domain, the flow of blood in vessels and arteries are pulsatile [42]. Thus, a user-defined function

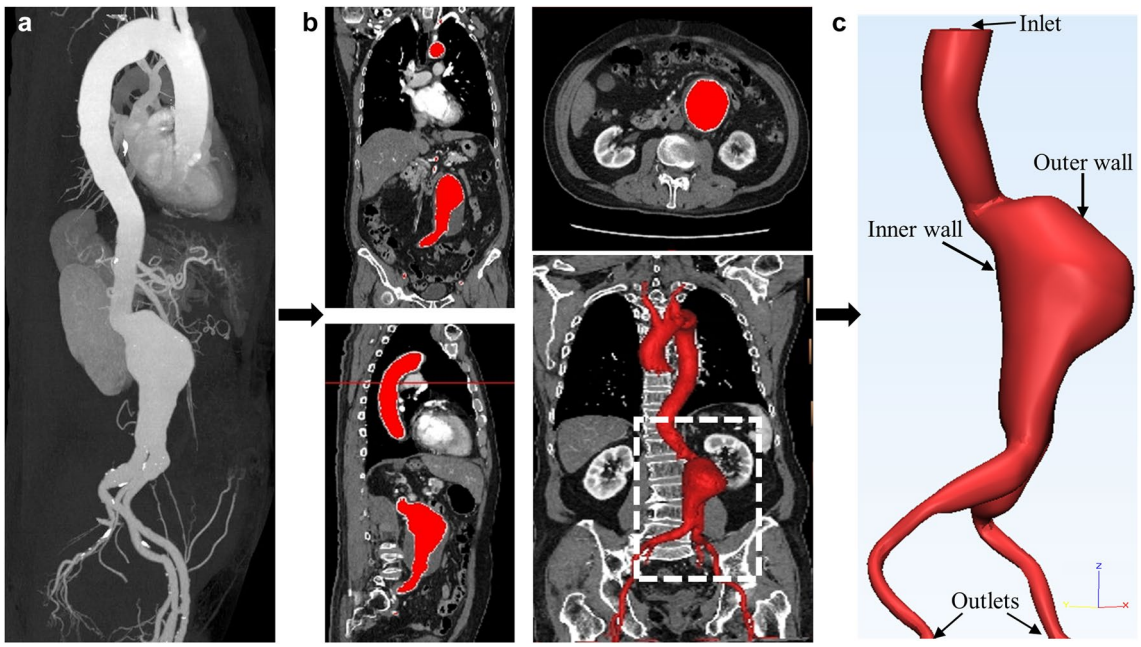

Fig. 1 Overall geometry reconstructions process, (a) CT image for the whole aorta, (b) the thresholding mask for aorta in the axial, coronal and sagittal view, and (c) 3D geometry for AAA after reconstruction, inner and outer walls are indicated by arrows to represent both side of abdominal aorta

(UDF) for a pulsatile velocity profile was used at the inlet for the whole cardiac pulse cycle with a velocity magnitude between 0 and 0.3 m/s as shown in Fig. 2. The inlet velocity profile was adopted from Rissland et al. [10]. For the outlet boundary, a fully developed outflow of a zero diffusion flux boundary condition was applied at the common iliac arteries [43]. A no-slip and rigid conditions for the arterial walls were assumed.

Simulation setup

All CFD transient simulations to solve the Navier–Stokes equations were carried out using ANSYS FLUENT v16.2 (ANSYS Inc., USA) under the shear stress transport k-omega (SST k-ω) turbulence model with a second order implicit method for transient formulations. The pressure–velocity coupling was set as SIMPLE algorithm to solve the continuity equation under 2nd order upwind momentum for spatial discretization. The convergence criteria for the normalized continuity and velocity residuals were 1×10^{-5}. A fixed time step of 0.01 s was used and three cardiac cycles (3×0.94 s) = 2.82 s or 282 time-steps were completed for each simulation.

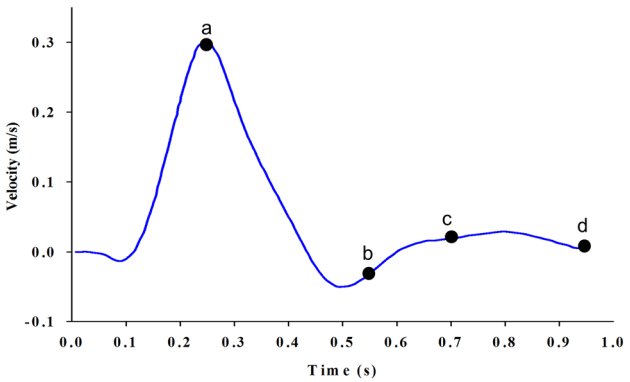

Fig. 2 Velocity waveform profile imposed at the inlet. (a) peak systole at 0.25 s; (b) early diastole 0.55 s; (c) mid diastole 0.70 s; and (d) late diastole 0.94 s

Results

The unsteady results of flow patterns (velocity contours in cross-sectional areas and streamlines) and WSS are presented at four different time points of a cardiac cycle indicated by the points in Fig. 2. These time-frames are (a) peak systole t = 0.25 s, (b) early diastole t = 0.55 s, (c) mid-diastole t = 0.70 s, and (d) late diastole t = 0.94 s. Table 2 presents the comparison of peak systolic velocity, early diastolic velocity, WSS and vorticity location between our work and previous studies that were performed on patient-specific geometries for healthy and diseased (AAA) abdominal aorta. Furthermore, additional data comparing a healthy artery and an angulated AAA is provided, along with a comparison of a laminar model and a turbulence model, and included as supplementary material.

Flow patterns

The velocity contours in regions of interest are presented in both horizontal and longitudinal cross-sectional areas as shown in Fig. 3(a). Four horizontal cross-sectional slides

Table 2 Comparison between present study and previous studies in terms of laminar and turbulence models for healthy abdominal aorta and abdominal aortic aneurysm (AAA) geometries

Study	Patient condition	CFD model	Velocity at peak systole (m/s)	Velocity at early diastole (m/s)	WSS (Pa)	Location of vorticity
Present study	AAA	Laminar[a]	3.32	0.40	2.12	Proximal neck, aneurysm sac and aortic bifurcation
		Turbulence	0.78	0.22	1.29	Proximal neck, aneurysm sac and aortic bifurcation
	Healthy[a]	Laminar	2.27	0.30	1.76	N/A
		Turbulence	2.17	0.25	2.67	N/A
Lozowy et al. 2017 [5]	AAA	Turbulence	0.4	0.15	1.5	Aneurysm sac
Sheidaei et al. 2011 [44]	AAA	Laminar	1.2	–	1.5	Aneurysm sac
Gur et al. 2017 [45]	Healthy	Laminar	1.13	0.25	15.0	No visualized vortices
Soudah et al. 2013 [46]	Healthy/AAA	Laminar	5.57/2.5	–	0.28/12.72[b]	No vortices/Aneurysm sac
Xenos et al. 2010 [47]	Healthy	Laminar	0.18	–	1.95	No vortices

[a]Supplementary material

[b]Mean WSS

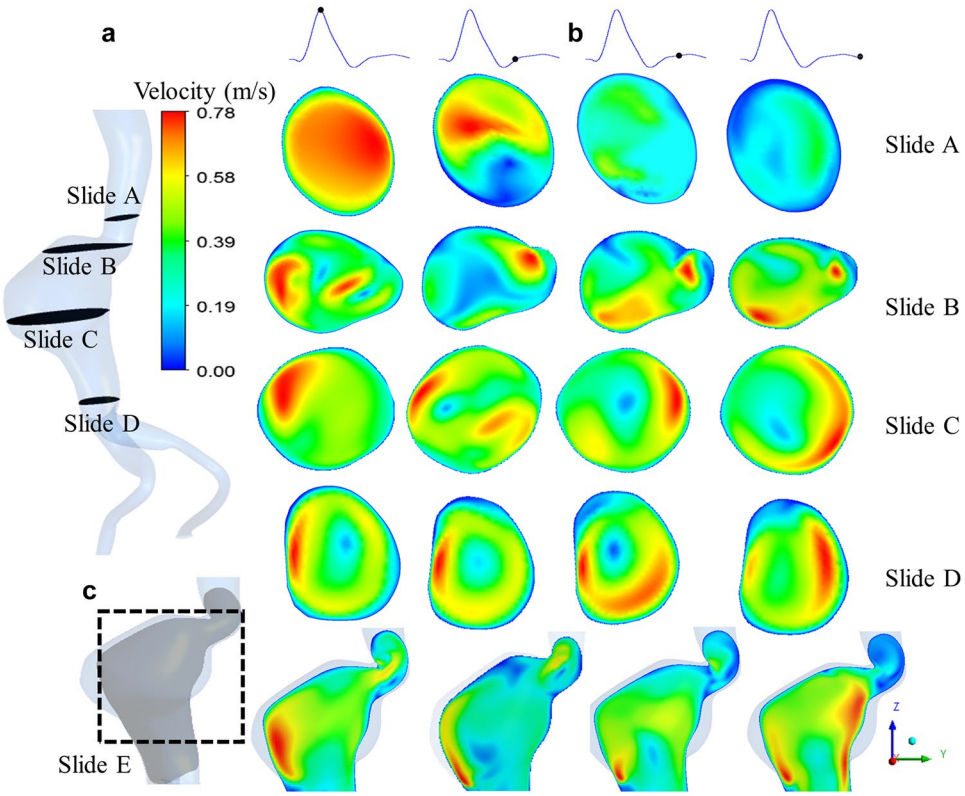

Fig. 3 Velocity contours at different horizontal cross-sectional areas for the angular neck AAA and aortic sac indicated by letters: **a** the four different locations in the geometry; **b** comparisons of the magnitude of the flow velocity at different time points in a cardiac cycle; **c** the vertical cross-sectional area of the model from proximal neck to lower region of sac

(A, B, D and C) in Fig. 3(b), and one longitudinal cross-sectional slide (E) extended from upper neck region towards the distal area of the sac as in Fig. 3(c). The contours of velocity within the horizontal cross-sectional slides show that the magnitude of velocity is significantly changed over the time. The maximum velocity at the peak systole clearly seems to be higher by approximately 55% than other maximum velocities over the different time points in a cardiac cycle, while velocity flow among the diastolic stages show similarity with slightly difference of only 4%. However, at all four time-points of a cardiac cycle the maximum blood flow occurs near the inner wall of the aorta, but cross-section of slide D views maximum blood flow near both inner and outer walls with local average velocity (0.15 m/s). The flows within slides C and D tend to form a circular shape within the aortic sac that can cause a high blood recirculation while maintaining a low velocity at the center of aorta with approximately 0.04 m/s.

Figure 3c emphasizes the velocity flow starting from upper the neck bending region towards the distal sac of aneurysm represented by the square box for the ROI. At a peak systolic time of 0.25 s, the velocity of flow entering the proximal neck of aneurysm towards the sac increased and led to an impingement of blood flow on the outer wall of aorta, subsequently diminishing through diastolic phase. At a full cardiac cycle of 0.94 s, high velocity flow is observed on both sides of the aneurysm sac which appears to coil up in this sectional view. The streamlines of velocity flows are presented in Fig. 4. The swirling of instantaneous velocity streamlines was acquired at different time points of a cardiac cycle as displayed in the ROI around the angular neck AAA. The recirculation blood vortexes are easily recognizable in various patterns over time.

WSS distribution

The WSS distribution of four different time points of a cardiac cycle configuration (peak systole, early diastole, mid diastole and late diastole) for high proximal neck angulation of AAA is depicted in Fig. 5. The WSS distributions are illustrated in three different views. View 1 and 2 show the WSS distribution at the regions of proximal aneurysm neck and view 3 illustrates the WSS distribution on the surface of aneurysm sac. We can observe that the high WSS of 1.24 Pa occurs at the area of proximal neck due to the turbulent flow exhibited within the region of angulation. The high bending, the severe tortuosity of aortic surface and asymmetric blood flow seem to be possible indicators of WSS and aortic rupture. At the peak systole and a fully developed cardiac cycle as in Fig. 6, high WSS regions are located at the areas below the angular neck and over the aneurysm sac as indicated by the red arrows with average value of 0.94 Pa, while the locations of low WSS with the average of 0.077 Pa are indicated by the black arrows. Furthermore, the values of WSS vary

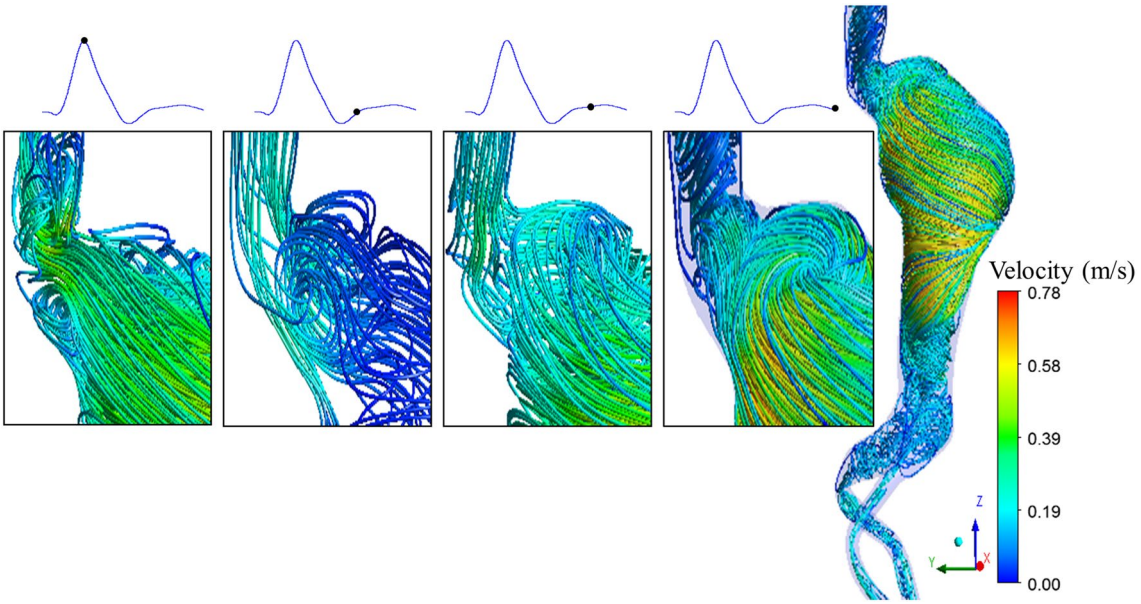

Fig. 4 Flow streamline contours at four different time points in a cardiac cycle

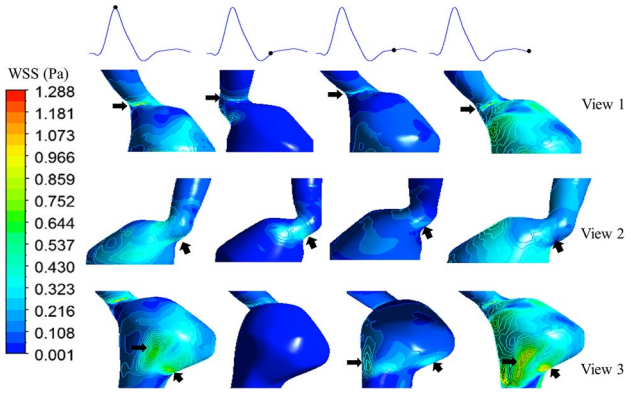

Fig. 5 WSS distribution on the angular neck and aneurysm sac regions at different time points in a cardiac cycle

between the healthy subject and AAA patients. In the AAA patients, WSS is lower than WSS in the healthy subjects as presented in Table 2.

Discussion

In this study, three-dimensional computational fluid dynamics simulations of a severe angulation neck of patient-specific AAA has been used to assess time-dependent hemodynamic. The three-dimensional geometry of angular neck AAA was reconstructed from computed tomography images. More specifically, the impact of high angular neck AAA on blood flow and wall shear stress (WSS) were assessed for an angle ($>60°$); particularly important due to the lack of studies in this area [22], where previous studies focused on smaller proximal angles ($\leq 60°$) or using idealized geometries [6, 17, 22, 43, 48].

Our study demonstrated the hemodynamic changes occur more pronounce at peak systole and turbulence flow was generated at the neck throughout the aneurysm sac during a cardiac cycle. In this study, the presence of a bending angle greater than 60° caused high flow turbulence and irregularities of blood-flow streamlines. This indicates that WSS and their distribution will be altered, with potential impact on weakening of arteries wall [43, 48].

The flow patterns at the systolic stage were observed to have complex and high velocity values within the proximal neck, while these maximum velocity values seemed to be decreased at the early and mid-diastole stages before it increased again at a complete cardiac cycle. As shown in Table 2, it is noted that the normal aorta model has higher peak systolic velocity than the AAA model. Vortex formation can be observed in geometries from AAA patients, whereas they cannot be observed in healthy aortas unless there is surface curvature, where only minimal recirculation may occur. The impact of proximal angular neck on blood flow within aneurysm sac was clearly showed to form a complex recirculation and flow impingement. This impact demonstrated a clear difference between the flow in AAA with an angulated proximal neck and without an angulated proximal neck. When the proximal neck is straight, the blood flows can be observed to follow laminar flow (i.e. not cross over streamlines) within the aneurysm sac with a very small region of recirculation [49]. It also showed that the velocity flow within the aorta was observed to have vorticity flow

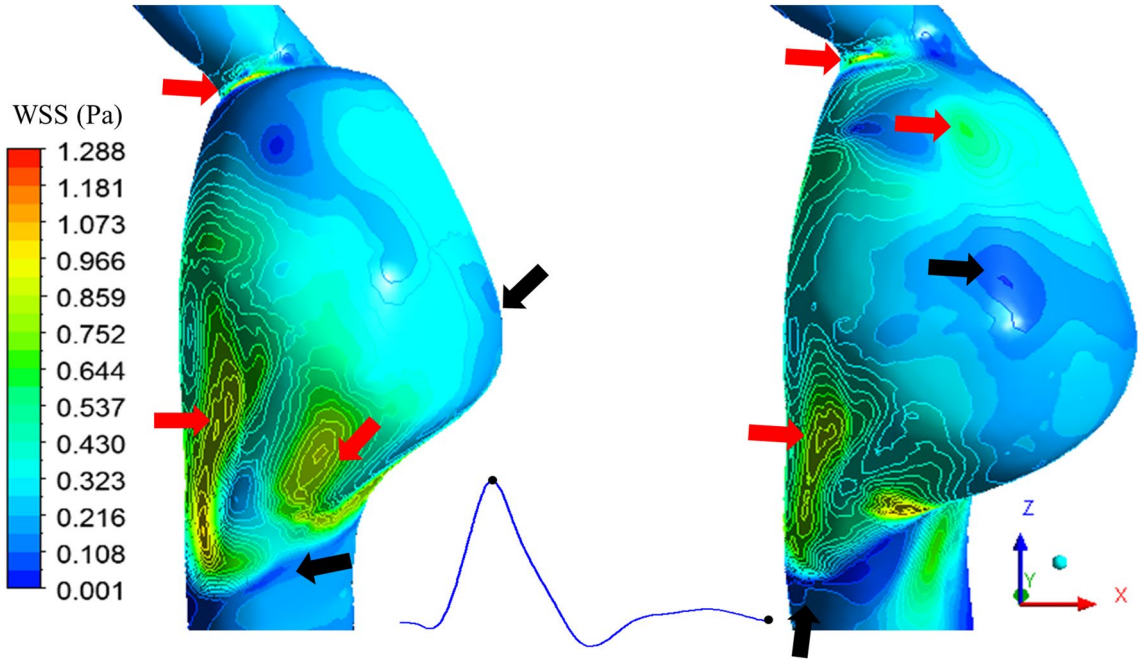

Fig. 6 WSS distribution for two time-points (0.25 s and 0.94 s) in a cardiac cycle. The high WSS regions are located with red arrows with average value of 0.94 Pa, while the locations of low WSS with the average of 0.077 Pa are indicated by the black arrows

and recirculation particularly through the aneurysm sac and aortic bifurcation, and these findings are consistent with idealized and real geometries in prior studies [31, 43, 48, 50], but our study reveals more complex recirculation and vorticity due to highly angulated neck and complexity of patient specific AAA geometry. Furthermore, a larger diameter for ruptured AAAs was associated with greater recirculation flow whereas less recirculation was found in smaller ruptured AAAs [51].

Several factors that influence the hemodynamic and the biomechanical conditions of arteries in cardiovascular system. For instance, vascular geometry, elasticity of the wall, blood viscosity and pathological conditions [52, 53]. Xenos et al. [17] conducted numerical simulations for 26 idealized geometries based on patient-specific data by using Fluid–Structure Interaction (FSI) simulations to investigate the effect of proximal necks ($40.10 \pm 16.30°$) in AAA. Correspondingly, Drewe et al. [6] studied similar range of neck angles in Xenos et al. [17] for idealized geometries in order to observe the stresses and hemodynamics. Both studies reported that peak WSS seems to be increased with the increase of proximal neck angles. However, the smaller angle of necks in their studies predicted peak WSS in the middle region of aneurysm sac due to the less turbulence of blood flow generated, while our findings with a larger neck showed WSS can be located more diffuse across areas such as below the proximal neck, middle of sac as well as at the lower side of the aneurysm sac wall. It has been reported that high WSS can promote endothelial injury, while low WSS can lead to inflammatory infiltration [54]. Therefore, this study has predicted a link between the behavior of blood flow and the change of WSS distribution. This correlation is consistent and demonstrates agreement with a previous study conducted by Arzani and Shadden [55].

The SST k − ω model was used in this study [50, 56]. According to Banks et al. [57] who found that this model was preferred for CFD turbulent flow simulations in arteries due to its better performances from other turbulence models when comparing the simulation outcomes against the results of experimental data. Furthermore, this turbulent model showed a good performance for the flow at boundary layers close to the wall, without applying a function of wall enhancement [57]. Therefore, it was observed that SST *k-ω* model was the most suitable method that provides better comparisons against the experimental results [58], it can be used for transitional flows for low Reynolds number. In addition, both laminar and turbulence models for AAA simulation show the formation of vortices within the aneurysm sac, which is similarly found in our study as presented in Table 2.

It should be noted that only one patient with a severe angular neck was studied. Following our study, we believe that it would be beneficial to increase the number of subjects to assess a wider range of proximal angular necks. However, this study demonstrates the effect of geometrical features based on a realistic time-varying velocity waveform, which is can be considered for personalized healthcare. It is appropriate

also to mention that this study implemented outflow boundary conditions at outlets which used the same waveform at the inlet of AAA section. This assumption is not expected to alter the overall findings as regards AAA neck angle and altered hemodynamics. Furthermore, it is worthy to point out that a possible thrombus was not included in this study. The presence of intraluminal thrombus (ILT) encourages the change of geometrical features that can consequently influence the biomechanics of AAA [59]. However, ILT was not involved in a scope of our study.

Conclusions

To summarize this work, the simulation concluded that the tortuosity of the aortic neck angulation causes a downstream of blood flow to be a turbulent flow and leads a weakening of the aortic wall, resulting in forming locations of high WSS. Thus, this study presented a comprehensive idea on the behavior of blood flow in highly angulated abdominal aortic aneurysm necks and its influence on wall shear stress. Furthermore, we recommend that more cases of patient-specific geometries are necessary to study the wider effect of angularity of the proximal neck on blood flow and subsequent hemodynamic changes in abdominal aortic aneurysm sac and aortic bifurcation.

Acknowledgements The authors wish to thank Mr. Sumrit Ruangchan and the radiology department, faculty of medicine, Prince of Songkla University for assisting with and providing the patient CT images, data and clinical suggestions.

Funding This study was funded by the Thailand's Education Hub for Southern Region of ASEAN Countries (TEH-AC) scholarship given to the Mr. Yousif A. Algabri and the thesis support funding from the graduate school, Prince of Songkla University. This work was also supported by a Researcher Links grant, ID 2017-RLTG8-10538, under the Newton-TRF Fund partnership. The grant is funded by the UK Department for Business, Energy and Industrial Strategy and Thailand Research Fund (TRF) (PDG61W0013) and delivered by the British Council.

Compliance with Ethical Standards

Conflict of interest The authors declare that they have no conflict of interest.

Ethical approval This article does not contain any studies with human participants or animals performed by any of the authors. Only images from patient-specific data were used in this study under the ethical approval acquired from Faculty of Medicine Ethics Committee, Prince of Songkla University under number REC.61-010-25-2.

References

1. Townsend N, Wilson L, Bhatnagar P, Wickramasinghe K, Rayner M, Nichols M (2016) Cardiovascular disease in Europe: Epidemiological update 2016. Eur Heart J 37:3232–3245. https://doi.org/10.1093/eurheartj/ehw334
2. Barquera S, Pedroza-Tobías A, Medina C, Hernández-Barrera L, Bibbins-Domingo K, Lozano R, Moran AE (2015) Global Overview of the Epidemiology of Atherosclerotic Cardiovascular Disease. Arch Med Res 46:328–338. https://doi.org/10.1016/j.arcmed.2015.06.006
3. Dua MM, Dalman RL (2010) Hemodynamic Influences on abdominal aortic aneurysm disease: Application of biomechanics to aneurysm pathophysiology. Vascul Pharmacol 53:11–21. https://doi.org/10.1016/j.vph.2010.03.004
4. Humphrey JD, Holzapfel GA (2012) Mechanics, mechanobiology, and modeling of human abdominal aorta and aneurysms. J Biomech 45:805–814. https://doi.org/10.1016/j.jbiomech.2011.11.021
5. Lozowy RJ, Kuhn DC, Ducas AA, Boyd AJ (2017) The Relationship Between Pulsatile Flow Impingement and Intraluminal Thrombus Deposition in Abdominal Aortic Aneurysms. Cardiovasc Eng Technol 8:57–69. https://doi.org/10.1007/s13239-016-0287-5
6. Drewe CJ, Parker LP, Kelsey LJ, Norman PE, Powell JT, Doyle BJ (2017) Haemodynamics and stresses in abdominal aortic aneurysms: A fluid-structure interaction study into the effect of proximal neck and iliac bifurcation angle. J Biomech 60:150–156. https://doi.org/10.1016/j.jbiomech.2017.06.029
7. Raut SS, Chandra S, Shum J, Finol EA (2013) The role of geometric and biomechanical factors in abdominal aortic aneurysm rupture risk assessment. Ann Biomed Eng 41:1459–1477. https://doi.org/10.1007/s10439-013-0786-6
8. Arzani A, Suh GY, Dalman RL, Shadden SC (2014) A longitudinal comparison of hemodynamics and intraluminal thrombus deposition in abdominal aortic aneurysms. Am J Physiol Circ Physiol 307:H1786–H1795. https://doi.org/10.1152/ajpheart.00461.2014
9. Ailawadi G, Eliason JL, Upchurch GR (2003) Current concepts in the pathogenesis of abdominal aortic aneurysm. J Vasc Surg 38:584–588. https://doi.org/10.1016/S0741-5214(03)00324-0
10. Rissland P, Alemu Y, Einav S, Ricotta J, Bluestein D (2009) Abdominal Aortic Aneurysm Risk of Rupture: Patient-Specific FSI Simulations Using Anisotropic Model. J Biomech Eng 131:31001. https://doi.org/10.1115/1.3005200
11. Kleinstreuer C, Li Z (2006) Analysis and computer program for rupture-risk prediction of abdominal aortic aneurysms. Biomed Eng Online 5:5–19. https://doi.org/10.1186/1475-925X-5-19
12. Li Z, Kleinstreuer C (2005) A new wall stress equation for aneurysm-rupture prediction. Ann Biomed Eng 33:209–213. https://doi.org/10.1007/s10439-005-8979-2
13. Böckler D, Holden A, Krievins D, de Vries JP, Peters AS, Geisbüsch P, Reijnen M (2016) Extended use of endovascular aneurysm sealing for ruptured abdominal aortic aneurysms. Semin Vasc Surg 29:106–113. https://doi.org/10.1053/j.semvascsurg.2016.09.002
14. Argani LP, Torella F, Fisher RK, McWilliams RG, Wall ML, Movchan AB (2017) Deformation and dynamic response of abdominal aortic aneurysm sealing. Sci Rep 7:17712. https://doi.org/10.1038/s41598-017-17759-3
15. de Bruin JL, Brownrigg JRW, Karthikesalingam A, Patterson BO, Holt PJ, Hinchliffe RJ, Morgan RA, Loftus IM, Thompson MM (2015) Endovascular aneurysm sealing for the treatment of ruptured abdominal aortic aneurysms. J Endovasc Ther 22:283–287. https://doi.org/10.1177/1526602815582529
16. Giuma SKB, Osman K, Kadir MRA (2013) Fluid structure interaction analysis in abdominal aortic aneurysms: Influence of diameter, length, and distal neck. J Med Imaging Heal Informatics 3:514–522. https://doi.org/10.1166/jmihi.2013.1201
17. Xenos M, Alemu Y, Zamfir D, Einav S, Ricotta JJ, Labropoulos N, Tassiopoulos A, Bluestein D (2010) The effect of angulation in

abdominal aortic aneurysms: Fluid-structure interaction simulations of idealized geometries. Med Biol Eng Comput 48:1175–1190. https://doi.org/10.1007/s11517-010-0714-y
18. Assar AN, Zarins CK (2009) Ruptured abdominal aortic aneurysm: A surgical emergency with many clinical presentations. Postgrad Med J 85:268–273. https://doi.org/10.1136/pgmj.2008.074666
19. Van Damme H, Sakalihasan N, Limet R (2005) Factors promoting rupture of abdominal aortic aneurysms. Acta Chir Belg 105:1–11
20. Wolf YG, Thomas WS, Brennan FJ, Goff WG, Sise MJ, Berntein EF (1994) Computed tomography scanning findings associated with rapid expansion of abdominal aortic aneurysms. J Vasc Surg 20:529–538. https://doi.org/10.1016/0741-5214(94)90277-1
21. Blanchard JF (1999) Epidemiology of abdominal aortic aneurysms. Epidemiol Rev 21:207–221. https://doi.org/10.1093/oxfordjournals.epirev.a017997
22. Sternbergh WC, Carter G, York JW, Yoselevitz M, Money SR (2002) Aortic neck angulation predicts adverse outcome with endovascular abdominal aortic aneurysm repair. J Vasc Surg 35:482–486. https://doi.org/10.1067/mva.2002.119506
23. Gray RA, Pathmanathan P (2018) Patient-Specific Cardiovascular Computational Modeling: Diversity of Personalization and Challenges. J Cardiovasc Transl Res 11:80–88. https://doi.org/10.1007/s12265-018-9792-2
24. Chaichana T, Sun Z, Jewkes J (2012) Investigation of the haemodynamic environment of bifurcation plaques within the left coronary artery in realistic patient models based on CT images. Australas Phys Eng Sci Med 35:231–236. https://doi.org/10.1007/s13246-012-0135-3
25. Morris PD, Narracott A, von Tengg-Kobligk H, Silva Soto DA, Hsiao S, Lungu A, Evans P, Bressloff NW, Lawford PV, Hose DR, Gunn JP (2016) Computational fluid dynamics modelling in cardiovascular medicine. Heart 102:18–28. https://doi.org/10.1136/heartjnl-2015-308044
26. Chung B, Cebral JR (2014) CFD for Evaluation and Treatment Planning of Aneurysms: Review of Proposed Clinical Uses and Their Challenges. Ann Biomed Eng 43:122–138. https://doi.org/10.1007/s10439-014-1093-6
27. Tseng FS, Soong TK, Syn N, Ong CW, liangb LH, Choongc AM (2017) Computational fluid dynamics in complex aortic surgery: applications, prospects and challenges. J Surg Simul 4:1–4. https://doi.org/10.1102/2051-7726.2017.0001
28. van Bakel TMJ, Lau KD, Hirsch-Romano J, Trimarchi S, Dorfman AL, Figueroa CA (2018) Patient-Specific Modeling of Hemodynamics: Supporting Surgical Planning in a Fontan Circulation Correction. J Cardiovasc Transl Res 11:145–155. https://doi.org/10.1007/s12265-017-9781-x
29. Prakobkarn A, Ina N, Saeheng S, Chatpun S (2017) Carotid artery stenosis pre-assessment by relationship derived from two-dimensional patient-specific model and throat velocity ratio. World J Model Simul 1:3–11
30. Carty G, Chatpun S, Espino DM (2016) Modeling Blood Flow Through Intracranial Aneurysms: A Comparison of Newtonian and Non-Newtonian Viscosity. J Med Biol Eng 36:396–409. https://doi.org/10.1007/s40846-016-0142-z
31. Owen B, Lowe C, Ashton N, Mandal P, Rogers S, Wein W, McCollum C, Revell A (2016) Computational hemodynamics of abdominal aortic aneurysms: Three-dimensional ultrasound versus computed tomography. Proc Inst Mech Eng Part H J Eng Med 230:201–210. https://doi.org/10.1177/0954411915626742
32. Raghavan ML, Vorp DA, Federle MP, Makaroun MS, Webster MW (2000) Wall stress distribution on three-dimensionally reconstructed models of human abdominal aortic aneurysm. J Vasc Surg 31:760–769. https://doi.org/10.1067/mva.2000.103971
33. del Álamo JC, Marsden AL, Lasherasa JC (2009) Recent Advances in the Application of Computational Mechanics to the Diagnosis and Treatment of Cardiovascular Disease. Rev Esp Cardiol 62:781–805. https://doi.org/10.1016/S1885-5857(09)72359-X
34. Fillinger MF, Marra SP, Raghavan ML, Kennedy FE (2003) Prediction of rupture risk in abdominal aortic aneurysm during observation: Wall stress versus diameter. J Vasc Surg 37:724–732. https://doi.org/10.1067/mva.2003.213
35. Di Martino ES, Vorp DA (2003) Effect of variation in intraluminal thrombus constitutive properties on abdominal aortic aneurysm wall stress. Ann Biomed Eng 31:804–809. https://doi.org/10.1114/1.1581880
36. Raghavan ML, Fillinger MF, Marra SP, Naegelein BP, Kennedy FE (2005) Automated Methodology for Determination of Stress Distribution in Human Abdominal Aortic Aneurysm. J Biomech Eng 127:868–871. https://doi.org/10.1115/1.1992530
37. Di Martino ES, Guadagni G, Fumero A, Ballerini G, Spirito R, Biglioli P, Redaelli A (2001) Fluid-structure interaction within realistic three-dimensional models of the aneurysmatic aorta as a guidance to assess the risk of rupture of the aneurysm. Med Eng Phys 23:647–655. https://doi.org/10.1016/S1350-4533(01)00093-5
38. Morbiducci U, Gallo D, Massai D, Consolo F, Ponzini R, Antiga L, Bignardi C, Deriu MA, Redaelli A (2010) Outflow conditions for image-based hemodynamic models of the carotid bifurcation: implications for indicators of abnormal flow. J Bomechanical Eng 132:91005. https://doi.org/10.1115/1.4001886
39. Gao F, Ohta O, Matsuzawa T (2008) Fluid-structure interaction in layered aortic arch aneurysm model: Assessing the combined influence of arch aneurysm and wall stiffness. Australas Phys Eng Sci Med 31:32–41. https://doi.org/10.1007/BF03178451
40. Scotti CM, Finol EA (2007) Compliant biomechanics of abdominal aortic aneurysms: A fluid-structure interaction study. Comput Struct 85:1097–1113. https://doi.org/10.1016/j.compstruc.2006.08.041
41. Frauenfelder T, Lotfey M, Boehm T, Wildermuth S (2006) Computational fluid dynamics: Hemodynamic changes in abdominal aortic aneurysm after stent-graft implantation. Cardiovasc Intervent Radiol 29:613–623. https://doi.org/10.1007/s00270-005-0227-5
42. Kao RH, Chen WL, Leu TS, Chen T, Kan CD (2014) Numerical Simulation of Blood Flow in Double-Barreled Cannon EVAR and its Clinical Validation. J Vasc Med Surg 2:160. https://doi.org/10.4172/2329-6925.1000160
43. Yeow SL, Leo HL (2016)Hemodynamic Study of Flow Remodeling Stent Graft for the Treatment of Highly Angulated Abdominal Aortic Aneurysm.Comput Math Methods Med 2016: 2016:3830123.https://doi.org/10.1155/2016/3830123
44. Sheidaei A, Hunley SCC, Zeinali-Davarani S, Raguin LG, Baek S (2011) Simulation of abdominal aortic aneurysm growth with updating hemodynamic loads using a realistic geometry. Med Eng Phys 33:80–88. https://doi.org/10.1016/j.medengphy.2010.09.012
45. Gur H, Ben, Brand M, Kósa G, Golan S (2017)Computational Fluid Dynamics of Blood Flow in the Abdominal Aorta Post "Chimney"Endovascular Aneurysm Repair (ChEVAR).In:Aortic Aneurysm.IntechOpen, pp 617–622
46. Soudah E, Ng EYK, Loong TH, Bordone M, Pua U, Narayanan S (2013) CFD modelling of abdominal aortic aneurysm on hemodynamic loads using a realistic geometry with CT. Comput Math Methods Med 2013. https://doi.org/10.1155/2013/472564
47. Xenos M, Rambhia SH, Alemu Y, Einav S, Labropoulos N, Tassiopoulos A, Ricotta JJ, Bluestein D (2010) Patient-based abdominal aortic aneurysm rupture risk prediction with fluid structure interaction modeling. Ann Biomed Eng 38:3323–3337. https://doi.org/10.1007/s10439-010-0094-3
48. Algabri YA, Rookkapan S, Chatpun S (2017) Three-dimensional finite volume modelling of blood flow in simulated angular

neck abdominal aortic aneurysm. IOP Conf Ser Mater Sci Eng 243:12003. https://doi.org/10.1088/1757-899X/243/1/012003
49. Finol EA, Keyhani K, Amon CH (2003) The Effect of Asymmetry in Abdominal Aortic Aneurysms Under Physiologically Realistic Pulsatile Flow Conditions. J Biomech Eng 125:207–217. https://doi.org/10.1115/1.1543991
50. Shek TLT, Tse LW, Nabovati A, Amon CH (2012) Computational Fluid Dynamics Evaluation of the Cross-Limb Stent Graft Configuration for Endovascular Aneurysm Repair. J Biomech Eng 134:121002. https://doi.org/10.1115/1.4007950
51. Boyd AJ, Kuhn DCS, Lozowy RJ, Kulbisky GP (2016) Low wall shear stress predominates at sites of abdominal aortic aneurysm rupture. J Vasc Surg 63:1613–1619. https://doi.org/10.1016/j.jvs.2015.01.040
52. Sinnott M, Cleary PW, Prakash M (2006)An investigation of pulsatile blood flow in a bifurcation artery using a grid-free method. In:Proc.Fifth International Conference on CFD in the Process Industries.Melbourne, pp 1–6
53. Gounley J, Vardhan M, Randles A (2017)A Computational Framework to Assess the Influence of Changes in Vascular Geometry on Blood Flow.In:Proceedings of the Platform for Advanced Scientific Computing Conference on -PASC'17.Lugano, pp 1–8
54. Dolan JM, Kolega J, Meng H (2013) High wall shear stress and spatial gradients in vascular pathology: A review. Ann Biomed Eng 41:1411–1427. https://doi.org/10.1007/s10439-012-0695-0
55. Arzani A, Shadden SC (2015) Characterizations and Correlations of Wall Shear Stress in Aneurysmal Flow. J Biomech Eng 138:14503. https://doi.org/10.1115/1.4032056
56. Tan FPP, Borghi A, Mohiaddin RH, Wood NB, Thom S, Xu XY (2009) Analysis of flow patterns in a patient-specific thoracic aortic aneurysm model. Comput Struct 87:680–690. https://doi.org/10.1016/j.compstruc.2008.09.007
57. Banks J, Bressloff NW (2007) Turbulence Modeling in Three-Dimensional Stenosed Arterial Bifurcations. J Biomech Eng 129:40–50. https://doi.org/10.1115/1.2401182
58. Ryval J, Straatman AG, Steinman DA (2004) Two-equation Turbulence Modeling of Pulsatile Flow in a Stenosed Tube. J Biomech Eng 126:625–635. https://doi.org/10.1115/1.1798055
59. Deplano V, Knapp Y, Bailly L, Bertrand E (2014) Flow of a blood analogue fluid in a compliant abdominal aortic aneurysm model: Experimental modelling. J Biomech 47:1262–1269. https://doi.org/10.1016/j.jbiomech.2014.02.026